INSTITUTE OF PHYSICS PUBLISHING JOURNAL OF PHYSICS B: ATOMIC, MOLECULAR AND OPTICAL PHYSICS

J. Phys. B: At. Mol. Opt. Phys. **35** (2002) 3729–3740 PII: S0953-4075(02)37290-0

Excitation of Ar^{15+} and Fe^{23+} for diagnostic application to fusion and astrophysical plasmas

A D Whiteford[1], N R Badnell[1], C P Ballance[2,3], S D Loch[1,4], M G O'Mullane[1] and H P Summers[1]

[1] Department of Physics, University of Strathclyde, Glasgow G4 0NG, UK
[2] School of Science and Mathematics, Sheffield Hallam University, Sheffield S1 1WB, UK

Received 21 May 2002, in final form 19 July 2002
Published 23 August 2002
Online at stacks.iop.org/JPhysB/35/3729

Abstract

Electron-impact excitation collision strengths for transitions among doubly excited levels up to the $n = 3$ shell (excluding the $1s3l3l'$ configurations) of lithium-like argon and iron have been calculated using a radiation- and Auger-damped, intermediate-coupling frame transformation, R-matrix approach. Collision strengths have also been calculated for transitions between all singly excited levels up to the $n = 5$ shell for the same systems.

The Maxwell-averaged effective collision strengths are estimated to be accurate to within 20% at temperatures 5×10^4–5×10^8 K for Ar^{15+} and 10^5–10^9 K for Fe^{23+}. These results are of substantially improved precision compared to previous studies.

The data relate to the analysis of soft x-ray helium-like spectra in both astrophysical and fusion thermal plasmas. We summarize the sensitivity to the new data of the spectral simulations which are matched to experiment in current spectral analysis procedures. Also, we present some brief results of modelling using the presented data.

1. Introduction

Experimental analysis procedures for soft x-ray spectra focus on the collections of spectrum lines (satellite lines) in the vicinity of the K_α resonance lines. Their theoretical description requires collisional and radiative data for both helium- and lithium-like systems (possibly also beryllium- and boron-like systems). These data must be compatible and of equivalent precision. For full exploitation of our recent work on collisional excitation of the helium-like systems of argon and iron (Whiteford *et al* 2001), we now wish to associate with it matching high-quality data for the corresponding lithium-like systems.

[3] Present address: Department of Physics, Rollins College, Winter Park, FL 32789, USA.
[4] Present address: Department of Physics, Auburn University, Auburn, AL 36849, USA.

Argon and iron have been chosen for this work, partly because of their importance in fusion and astrophysical plasmas, but also because they display the range of advanced collisional aspects now recognized as necessary to obtain high-precision cross-sections.

In magnetic confinement fusion, argon is a species of choice for the modification of edge conditions (via transport barriers etc) by radiative cooling and this has led to the decision by the fusion community to establish argon as a reference species. Diagnostic experiments are planned at the EFDA–JET facility to compare and evaluate measured argon spectra against modelled emission. Also, the International Atomic Energy Agency (IAEA) has established a diagnostics collaborative research proposal (CRP), of which the assembly of argon electron-impact data is a part. Spectroscopic deduction of argon concentrations uses core observations of the helium- and lithium-like ionization stages. Such deduction exploits the soft x-ray along with visible lines of charge exchange spectroscopy. The high-quality atomic data presented here are part of the theoretical input to these activities.

High-resolution soft x-ray spectra of both argon and iron are measured at the TEXTOR tokamak. A significant concentration of thermal neutral hydrogen can penetrate to the core of the plasma in this device. The familiar helium-like resonance line spectral vicinities show small modifications of relative intensities as discussed in the case of argon by Rosmej *et al* (1999). These modifications are believed to be due to the disturbing effect of charge exchange from the thermal neutral hydrogen on the conventional electron-impact-driven emission. The separation of these effects places a high demand for accuracy on the electron-impact collision cross-section calculations. Current studies on the same effect in iron are being performed by Bertschinger at TEXTOR.

In the astrophysical domain, high-resolution soft x-ray spectra of iron from solar flares have been observed for many years (cf SMM and YOKHOH satellites). Soft x-ray emission from cosmological objects is now observed with unprecedented resolution by the *Chandra* and *XMM–Newton* spacecraft. Astrophysical phenomena such as galactic cooling flows and accretion columns around black holes show soft x-ray emission of iron, but often in contrasting excitation conditions. The differences between low-density photoionized environments and the higher-density collisionally ionized environments warrant the incorporation of more sophisticated data. The RmaX network, whose focus is on both electron- and photo-induced x-ray transitions, was partly established to support *Chandra* observations. The results presented here form part of the RmaX network.

Recent work by Ballance *et al* (2001) addressed the key problematic issues of highly charged lithium-like ions. The importance of inner-shell processes of Fe^{23+} using the *R*-matrix method was appraised and special consideration was given to radiation damping for the doubly excited transitions. Following this pilot study by Ballance *et al* (2001), and in light of present computing power, it is appropriate to address a complete calculation for lithium-like ions. The present calculations include radiation and Auger damping (Auger damping was not considered by Ballance *et al* (2001)) and extend to all 4005 transitions that arise between doubly excited levels up to the $n = 3$ shell (excluding $1s3l3l'$ levels) in an intermediate-coupling picture. They also encompass the 276 transitions between all singly excited levels up to the $n = 5$ shell. The inclusion of Auger damping for doubly excited transitions gives a significant difference from the work of Ballance *et al* (2001) for a number of transitions.

The effects of Auger damping have been studied extensively for electron-impact ionization of lithium-like ions by a number of authors including Tayal and Henry (1991) and Chen and Reed (1992). Badnell and Pindzola (1993) studied the electron impact excitation of few-electron highly charged ions and discussed Auger breakup and its effect on resonance contributions.

Merts *et al* (1980) presented (unreferenced) excitation data for a number of ions including data by Mann, Younger and Sampson for Ar^{15+} and data by Mann, Eissner, Hummer, Pindzola and Dufton for Fe^{23+}. However, these data were only presented in LS form, i.e. the transitions were between terms and not levels.

Goett and Sampson (1983) calculated collision strengths for the $1s^2 2l$–$1s2l'2l''$ transitions for all ions with $6 \leqslant Z \leqslant 74$ using a distorted-wave approach; this was an extension of their work (Goett *et al* 1984) which calculated data for the same transitions for only lithium-like Si, Ca, Fe, Kr and Gd ions[5].

Sampson *et al* (1985a, 1985b) went on to calculate core-excited distorted wave collision strengths for the $1s^2 2l$–$1s2l2l'$ (1985a) and the $1s^2 3l$–$1s2l'3l''$ (1985b) transitions, of all ions with $6 \leqslant Z \leqslant 74$, with Zhang *et al* (1986) producing data for all transitions occurring within the levels of the $1s^2 2l2l'$ configurations of the same ions.

Zhang *et al* (1990) published data using a distorted-wave approach for all ions with $8 \leqslant Z \leqslant 92$ and calculated outer-shell electron-impact collision strengths between the levels of the $n = 2$ shell and from these levels up to the $n = 5$ shell. Transitions between excited states of the $n = 3, 4, 5$ shell were not calculated, resonances were neglected and effective collision strengths were not generated.

Berrington and Tully (1997) performed calculations for the outer-shell excitation rates up to the $n = 4$ shell of Fe^{23+} using an R-matrix approach as part of the iron project (Hummer *et al* 1993). They published effective collision strengths between 1.6×10^6 and 10^8 K, highlighting the importance of the resonance contribution (particularly in the $1s^2 2p\ ^2P_{\frac{1}{2}}$–$1s^2 2p\ ^2P_{\frac{3}{2}}$ transition) by comparing with the earlier distorted-wave work of Zhang *et al* (1990). They only presented data for collisions which included levels within the ground configuration.

The structure of this paper is as follows: in section 2 we discuss the details of our collision strength calculations and present some illustrative results and comparisons. In section 3 we make some comparisons of our effective collision strengths with those of other workers; we also discuss the application of our data to collisional–radiative modelling and briefly present some modelling results. We finish with a short conclusion.

2. Calculations and results

2.1. Methodology

Our approach to the determination of the collision strengths is to use the R-matrix method (Burke and Berrington 1993) in conjunction with the intermediate-coupling frame transformation (ICFT) method (Griffin *et al* 1998) and the optical potential approach to radiation and Auger damping (Robicheaux *et al* 1995, Gorczyca and Badnell 1996, Gorczyca and Robicheaux 1999).

Use is made of multi-channel quantum defect theory (MQDT) to obtain 'unphysical' collision matrices (as implemented by Gorczyca and Badnell (2000)). The outer region solutions include the long-range coupling potentials as a perturbation, still within the MQDT framework (see Gorczyca *et al* 1996, Badnell and Seaton 1999).

Our approach to the inner- and outer-shell data is to perform the calculations independently and later merge the effective collision strengths back together into a single dataset because this cuts down on the size of Hamiltonians to diagonalize and the number of transitions to process.

[5] The publication (Goett *et al* 1984) focusing only on limited ions was published after the publication (Goett and Sampson 1983) on all ions with $6 \leqslant Z \leqslant 72$ even though the latter was based on the methodology of the former.

Table 1. Energy levels (cm^{-1}) of Ar^{15+} and Fe^{23+}, up to $n = 3$ for all singly excited levels and selected (representative) levels from higher singly and doubly excited states.

	Ar^{15+}		Fe^{23+}	
Level	Present	NIST[a]	Present	NIST
$1s^2 2s\ ^2S_{\frac{1}{2}}$	0	0	0	0
$1s^2 2p\ ^2P_{\frac{1}{2}}$	257 755	257 026	392 591	392 000
$1s^2 2p\ ^2P_{\frac{3}{2}}$	283 159	282 603	520 041	520 720
$1s^2 3s\ ^2S_{\frac{1}{2}}$	4 177 981	4 176 030	9 276 233	9 272 400
$1s^2 3p\ ^2P_{\frac{2}{2}}$	4 249 034	4 246 460	9 384 701	9 378 000
$1s^2 3p\ ^2P_{\frac{3}{2}}$	4 256 554	4 254 050	9 421 775	9 417 000
$1s^2 3d\ ^2D_{\frac{3}{2}}$	4 284 176	4 281 170	9 465 645	9 459 000
$1s^2 3d\ ^2D_{\frac{5}{2}}$	4 286 540	4 283 560	9 477 659	9 472 000
$1s^2 4s\ ^2S_{\frac{1}{2}}$	5 608 169	5 605 740	12 469 633	12 464 000
$1s^2 5s\ ^2S_{\frac{1}{2}}$	6 262 964	6 259 500	13 935 076	—
$1s2s^2\ ^2S_{\frac{1}{2}}$	24 879 049	24 834 000	53 340 361	—
$(1s2s\ ^3S)2p\ ^2P_{\frac{1}{2}}$	25 148 657	31 333 000[b]	53 757 894	53 657 000
$(1s2s\ ^3S)2p\ ^2P_{\frac{3}{2}}$	25 161 992	31 342 000[b]	53 834 716	53 752 000

[a] NIST database (http://physics.nist.gov/).
[b] We believe these values to be incorrect—see text for details.

2.2. The atomic structure calculations

We used AUTOSTRUCTURE (Badnell 1997) to calculate the atomic structure and, hence, to generate radial wavefunctions for the collision calculation. Table 1 summarizes the energy-level results in comparison with those of NIST (2001). The energies given for the $(1s2s\ ^3S)2p\ ^2S_{\frac{1}{2},\frac{3}{2}}$ levels should not be confused with the results of Ballance *et al* (2001, table 1) as they presented energies for the $(1s2s\ ^3S)2p\ ^4S_{\frac{1}{2},\frac{3}{2}}$ levels but they did not specify the term or parentage in their table[6].

We note that we have a strong disagreement with NIST for the $1s2s2p\ ^2S_{\frac{1}{2},\frac{3}{2}}$ levels of Ar^{15+}. We find disagreements of a similar magnitude between the present work and NIST for all doubly excited energy levels of Ar^{15+}, with the exception of the $1s2s^2\ ^2S_{\frac{1}{2}}$ level. The energy of the $(1s2s\ ^3S)2p\ ^2P_{\frac{1}{2}}$ level as given by Goett and Sampson (1983) is 25 116 613 cm^{-1} which is in much closer agreement with the present work than with NIST. We note that the NIST data disagree with the data of Kelly (1987) which is the publication NIST references for its argon data. We conclude that the NIST energy levels for doubly excited states of Ar^{15+} are in error[7].

2.3. Auger damping

The damping of resonances due to Auger breakup is dealt with in two distinct cases. The first case is for the Auger breakup to states included explicitly in the calculation; this case is dealt with within the *R*-matrix approach intrinsically. The second case is for Auger breakup to states not included in the close-coupling expansion. In this latter case, we use AUTOSTRUCTURE

[6] It is noted that term and parentage assignment is breaking down and the *LS* coupled labelling scheme is used as a convenience.

[7] We also note that the energies NIST quote for Ar^{15+} are very close to the energies of the corresponding states in (lithium-like) Ca^{17+}.

to calculate Auger widths for the core re-arrangement of each target level and include them in the optical potential in our outer-region calculation.

As an example, consider the $1s^2 2s\ ^2S_{\frac{1}{2}}$–$1s2s^2\ ^2S_{\frac{1}{2}}$ transition. This will have near-threshold resonances corresponding to 1s2s2pnl states. The core re-arrangement Auger damping of such intermediate states to $1s^2nl + e^-$ for $n > 3$ (in our case) is not included explicitly in the R-matrix calculation. We can represent this schematically by

$$\begin{array}{ccccc} 1s^2 2s + e^- & \rightleftharpoons & 1s2s2pnl & \rightarrow & 1s2s^2 + e^- \\ & & \swarrow \quad \searrow & & \\ & & 1s^2 2p + e^- \quad 1s^2 nl + e^-. & & \end{array}$$

The $\leftharpoondown$ and $\swarrow$ Auger pathways scale as n^{-3} while the $\searrow$ route is independent of n and thus dominates for sufficiently high n.

To calculate the Auger width of such a process we consider the Auger breakup of the three-electron system going from 1s2s2p to $1s^2 + e^-$. This neglects the effect of the spectator nl electron on the core N-electron Auger breakup. We then incorporate the Auger width into the optical potential approach to damping as discussed by Gorczyca and Robicheaux (1999) for the case of Auger damping following photoexcitation.

For the case of the $1s^2 2s\ ^2S_{\frac{1}{2}}$–$1s2s^2\ ^2S_{\frac{1}{2}}$ transition in Fe^{23+}, only resonances with $n \geqslant 10$ are above threshold (Chen and Reed 1992) and so none of these would be (core re-arrangement) Auger damped in a standard R-matrix calculation. A rigorous analysis of the effects of such Auger damping on the $1s^2 2s\ ^2S_{\frac{1}{2}}$–$1s2s^2\ ^2S_{\frac{1}{2}}$ transition is presented when we discuss our effective collision strengths.

2.4. The collisional calculations

The inner-region solutions were obtained using R-matrix codes which are based upon the published exchange codes of Berrington *et al* (1995) and the non-exchange codes of Burke *et al* (1992). The outer-region solutions, including radiation damping, were obtained in an LS-coupling scheme using the code STGFDAMP and the intermediate-coupling frame transformation was applied using the code STGICFDAMP, which included the effect of Auger damping not already included explicitly by the R-matrix method. At high angular momenta and/or energies, no resonances are resolved and/or present and it is more efficient to use the undamped versions of these codes, namely STGF and STGICF.

For the inner-shell calculation, we used 30 continuum basis orbitals per angular momentum within the exchange R-matrix codes. The non-exchange R-matrix codes reduce this number progressively as the continuum orbital angular momentum increases. Accurate collision strengths can be generated for electron energies up to between half and three-quarters of the smallest maximum basis-orbital energy. The smallest maximum basis orbital energy corresponds to ≈1116 Ryd in the case of Ar^{15+} and ≈2445 Ryd in the case of Fe^{23+}; the smallest maximum basis orbital occurred for the $L = 3$ partial wave in both ions. For the outer-shell calculation, we used 80 continuum basis orbitals per angular momentum within the exchange R-matrix codes which gave smallest maximum basis orbital energies of ≈1567 for Ar^{15+} and ≈3515 in the case of Fe^{23+}. Both of these minima occurred for the $L = 5$ partial wave.

The exchange calculation was performed up to $J = 10$ and the non-exchange calculation up to $J = 58$. After that, 'top-up' was used to complete the partial collision strength sum over higher values of J. The top-up for non-dipole transitions was calculated by assuming a geometric series in energy, but taking care to switch over smoothly to the degenerate-energy limiting case (Burgess *et al* 1970). The top-up for dipole transitions was computed using the Burgess (1974) sum rule.

We took care to resolve the dominant resonance structure. In the case of both Ar^{15+} and Fe^{23+}, we used an energy mesh of $1 \times 10^{-5} z^2$ Ryd (z being the ionic charge) below the last threshold and a mesh of $1 \times 10^{-3} z^2$ Ryd above the last threshold (i.e. in the resonance-free region). This energy mesh resolves the resonance structure in the detail necessary to generate reliable effective collision strengths as illustrated in the sensitivity studies of Badnell and Griffin (2001) and Whiteford *et al* (2001). We note that the incorporation of radiation and Auger damping at the heart of our approach both reduces and broadens the (damped) resonances that we need to resolve. Hence, our effective resolution is greater than that of an initially undamped calculation that uses an equivalent energy mesh, as is done in the resonance-fitting approach to the damping of low-n resonances (Sakimoto *et al* 1990).

We follow closely the methodology used by Ballance *et al* (2001) but we perform the calculation with the express intention of making it directly applicable to application. Ballance *et al* (2001) used a combination of Breit–Pauli (BP) (up to $J = 4$) and ICFT (from $J = 5$ to 28) and then used top-up to complete their calculation. We instead choose to perform an exclusively ICFT exchange calculation up to $J = 10$ and then use it with the non-exchange codes of Burke *et al* (1992) for $J = 11$–58 in order to increase efficiency for the intermediate partial waves (i.e. $J = 11$–28) and also to give a higher-quality cross section for the higher partial waves (i.e. $J = 29$–58). We choose to use more continuum basis orbitals so that we can produce more accurate collision strengths at higher energies and we have also used a four-times-finer energy mesh so that we can be confident the resonances are sufficiently resolved for the integration to produce effective collision strengths. Ballance *et al* (2001) neglected the effects of Auger damping, which we show here to be important for low-temperature effective collision strengths.

2.5. Results

For each system, our inner-shell calculations yield effective collision strengths for 4005 transitions and the outer shell calculations yield effective collision strengths for 276 transitions (with 28 transitions overlapping between the two cases) and so only illustrative results are presented here. The full set of merged inner- and outer-shell results, for both Ar^{15+} and Fe^{23+}, for energy levels, radiative rates, infinite-energy Born collision strengths and (Maxwell-averaged) effective collision strengths has been compiled according to the requirements of the Atomic Data and Analysis Structure (ADAS) Project (data format *adf04*) (Summers 1994, 1999) and is available via the world-wide web[8]. The tabulated temperature range of the effective collision strengths is 5×10^4–5×10^8 K for Ar^{15+} and 10^5–10^9 K for Fe^{23+}. Where there were data available from both calculations, we opted to use the data from the singly excited calculation since the effect of resonances attached to levels of the $n = 4$ and 5 shells is more important to singly excited effective collision strengths than the effect of resonances attached to doubly excited levels.

The *adf04* data format is a compact and useful way of archiving the present data so that it can be directly applied to plasma analysis with little inconvenience on the part of the modeller. Care has been taken to ensure the dataset is complete, including, e.g., non-dipole radiative rates which are often not generated. For the case of a dataset containing 4253 transitions, it is non-trivial for a modeller to separately obtain or calculate radiative rates and insert them into the dataset since even a very slightly different structure will cause the re-ordering of levels. For the case of Ar^{15+}, 1968 non-dipole (M1/E2) radiative rates were included.

Figure 1 shows a comparison of a dipole transition, $1s^2 2s\ ^2S$–$1s^2 2p\ ^2P$ in Ar^{15+}, with the data presented by Merts *et al* (1980). The plot is presented in the 'C-plot' of Burgess and Tully

[8] Available from the Controlled Fusion Atomic Data Center, Oak Ridge, USA—http://www-cfadc.phy.ornl.gov/data_and_codes.

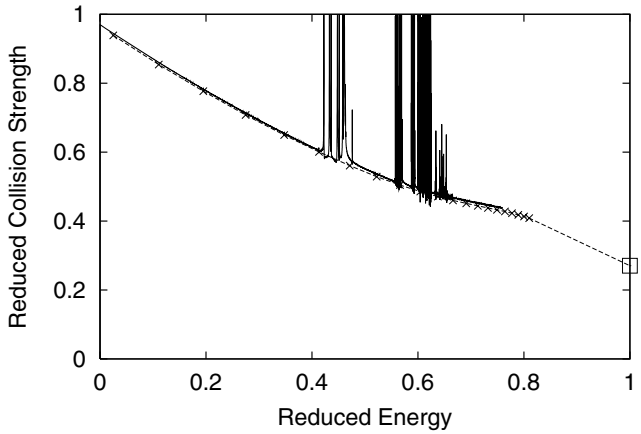

Figure 1. Reduced electron-impact excitation collision strengths for the $1s^2 2s\ ^2S$–$1s^2 2p\ ^2P$ transition in Ar^{15+} obtained using a reduced-energy parameter of $C = 3$. The solid curve denotes the present results and shows the detailed resonance structure. The dashed curve and crosses denote the distorted-wave results presented by Merts *et al* (1980). The straight line between the last point of Merts and the infinite-energy limit point (square box) shows the approach to the limit point.

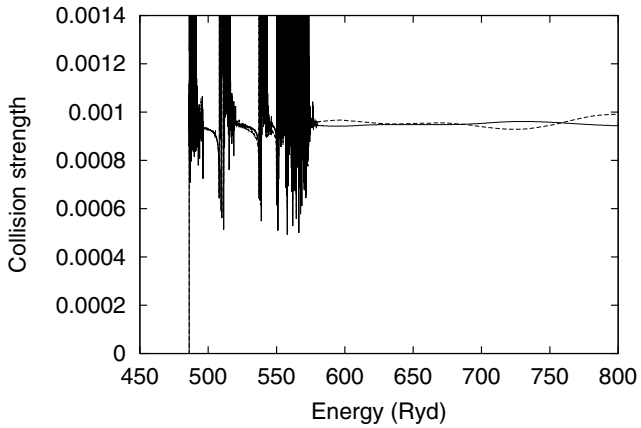

Figure 2. Electron-impact excitation collision strengths for the $1s^2 2s\ ^2S_{\frac{1}{2}}$–$1s2s^2\ ^2S_{\frac{1}{2}}$ transition in Fe^{23+}. The solid curve denotes the present work and the dashed curves the work of Ballance *et al* (2001).

(1992). Note that in order to make the comparison we show our LS coupled results before they were transformed to IC coupling using the ICFT approach.

Figure 2 shows a comparison between the current work and the work of Ballance *et al* (2001) in the $1s^2 2s\ ^2S_{\frac{1}{2}}$–$1s2s^2\ ^2S_{\frac{1}{2}}$ transition of Fe^{23+}. Note the shallow oscillations in the background collision strength (well outside the resonance region) in the work of Ballance *et al* (2001) since they used fewer basis orbitals than the present work. It can be seen, however, that the collision strengths of Ballance *et al* (2001) are oscillating around the collision strengths of the present work. Upon integration to form effective collision strengths the over- and under-estimations will tend to cancel each other out, but such a cancellation is best avoided if possible.

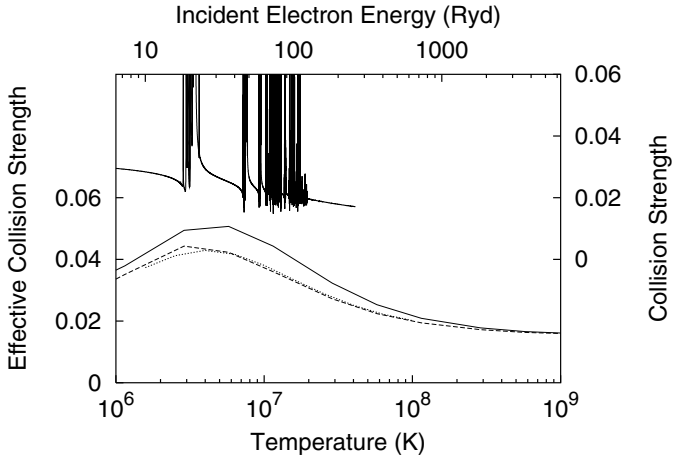

Figure 3. Effective collision strengths for the $1s^2 2p\ ^2P_{\frac{1}{2}}$–$1s^2 2p\ ^2P_{\frac{3}{2}}$ transition of Fe^{23+}. The solid curve shows the effective collision strength including resonances attached to $n = 3, 4$ and 5 states, the dashed curve shows the results with resonance contribution coming only from resonances attached to $n = 3$ states. Also shown (dotted curve) are the results of Berrington and Tully (1997). The solid curve above the effective collision strengths is the underlying collision strength. The energy and temperature ordinates are scaled according to $E = kT$.

3. Application of fundamental data

3.1. Effective collision strengths

The collision strengths were Maxwell averaged, using the approach of Burgess *et al* (1997), to generate effective collision strengths for spectral analysis and modelling. The collision strengths for allowed transitions were interpolated at higher energies using the infinite-energy limit points in the 'C-plot' picture. The collision strengths for forbidden transitions were extrapolated by assuming an $E^{-\alpha}$ energy dependence, with $\alpha = 1$–2. Formally (Burgess and Tully 1992), an E^{-2} energy dependence is expected. The details of our interpolation and extrapolation are discussed in more detail by Whiteford *et al* (2001).

In figure 3, we display the importance of including enhancement due to resonances attached to levels in the $n = 4$ and 5 shells in the $1s^2 2p\ ^2P_{\frac{1}{2}}$–$1s^2 2p\ ^2P_{\frac{3}{2}}$ transition of Fe^{23+}. A comparison with Berrington and Tully (1997), who included the effects of resonances attached to levels up to the $n = 4$ shell, is also shown. While the position of the resonance enhancement of the effective collision strength is at the same place, the results themselves differ somewhat when we include resonances attached to $n = 4$ and 5 shells. We note that Berrington and Tully (1997) have closer agreement with our results for inclusion of resonances up to the $n = 3$ shell even though they also included resonances attached to the $n = 4$ shell.

In figure 4, the effect of Auger damping not included in a standard R-matrix calculation is illustrated at low temperatures for the $1s^2 2s\ ^2S_{\frac{1}{2}}$–$1s2s^2\ ^2S_{\frac{1}{2}}$ transition in Fe^{23+}. The effective collision strength at low temperatures is dominated by the resonances corresponding to the 1s2s2pnl $(N + 1)$ electron states. Such intermediate states have a high rate of Auger breakup to $1s^2 nl + e^-$ and, hence, the resonances are damped almost completely. The breakdown of the contributions to the effective collision strength is given in table 2 for a range of different temperatures. As would be expected, the resonance contribution is large at low temperature, but the full inclusion of Auger damping reduces this contribution greatly.

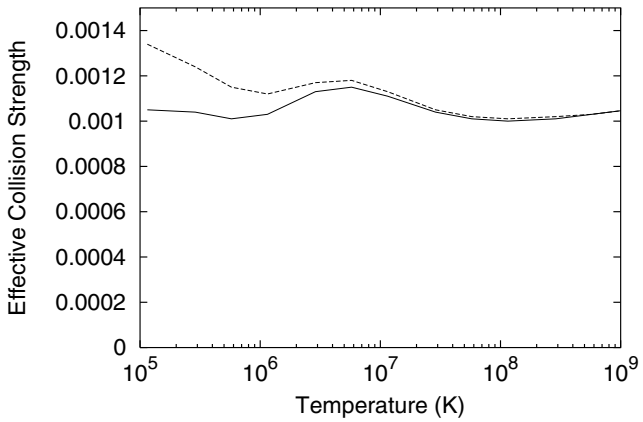

Figure 4. Effective collision strengths for the $1s^2 2s\ ^2S_{\frac{1}{2}}$–$1s2s^2\ ^2S_{\frac{1}{2}}$ transition of Fe^{23+}. The solid curve shows the effective collision strength including the effects of Auger damping not included in a standard R-matrix calculation. The dashed curve shows the results neglecting the effects of such Auger damping.

Table 2. Contributions to the effective collision strength (divided by 10^{-4}) of the $1s^2 2s\ ^2S_{\frac{1}{2}}$–$1s2s^2\ ^2S_{\frac{1}{2}}$ transition in Fe^{23+} showing contributions with full Auger damping included (ADI) and excluded (ADE) (see the text for details).

Temperature (K)	3×10^5		3×10^6		3×10^7		3×10^8	
Contribution	ADI	ADE	ADI	ADE	ADI	ADE	ADI	ADE
Background	9.48		9.49		9.51		10.0	
1s2s2pnl	0.92	2.92	0.05	0.47	—[b]	0.02	—	—
1s2s3l3l'	—	—	1.41	1.41	0.49	0.49	0.01	0.01
1s2s3l4l'	—	—	0.11	0.13	0.20	0.22	0.01	0.01
1s2s3l5l'	—	—	0.09	0.09	0.24	0.26	0.01	0.01
1s2s3nl'[a]	—	0.11	—	—	0.02	0.69	—	0.01
Total	10.4	12.5	11.1	11.6	10.4	11.2	10.0	10.0

[a] $n \geqslant 6$.
[b] — denotes negligible contribution.

At a temperature of 10^6 K in Fe^{23+}, effective collision strengths for ∼750 transitions are overestimated by $\gtrsim$30% if Auger damping is neglected, with the worst case being a factor of ∼9 overestimate in the 1s2s3s $^2S_{\frac{1}{2}}$–1s2p3p $^2P_{\frac{1}{2}}$ transition.

We find broad accord with the effective collision strengths calculated by Ballance *et al* (2001)[9] for a number of representative transitions and temperature ranges where Auger damping does not have a significant effect.

3.2. Population modelling

For application, the present resultant rate coefficients must be incorporated into excited population models. We used the collisional–radiative codes of the Atomic Data and Analysis Structure (ADAS) for our analysis (Summers 1994, 1999).

[9] We note that table 3 of Ballance *et al* (2001) is in error; we compared with the *adf04* dataset produced by Ballance *et al* (2001) and not to table 3.

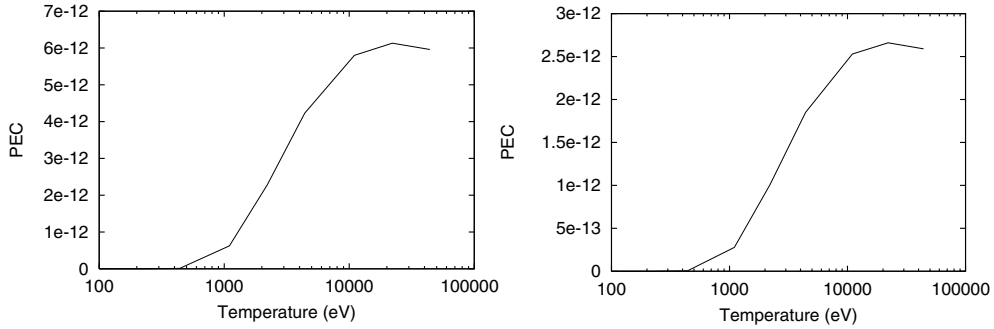

Figure 5. $\mathcal{PEC}$s for the $1s^2 2s\ ^2S_{\frac{1}{2}}$–$1s2s2p\ ^2P_{\frac{3}{2}}$ (left plot) and $1s^2 2s\ ^2S_{\frac{1}{2}}$–$1s2s2p\ ^2P_{\frac{1}{2}}$ (right plot) transitions (corresponding to the q and r lines, respectively) in Ar^{15+} as a function of temperature for a density of 10^{13} cm^{-3}.

We note that, for the first part of our analysis, we are only considering collisional excitation processes and neglecting the effects of recombination on the population structure and emission; this is a poor assumption if one is to do modelling of the emission of the considered systems under typical fusion and astrophysical conditions. However, neglecting recombination allows us to focus on the excitation part alone and investigate the temperature dependence and sensitivity to errors without the issues being clouded by recombination. There do exist several lines which come from upper levels which are primarily populated by inner-shell excitation; the accurate determination of these populations is a major focus of the present rate coefficient calculation since any errors in the populations will be mostly due to electron-impact excitation data and not recombination data.

We used the code ADAS208 to construct and solve the collisional–radiative matrices for the lithium-like system so as to give us excited-state population dependences[10]. Further, we used ADAS208 to calculate photon emissivity coefficients ($\mathcal{PEC}$s). The computed $\mathcal{PEC}$s are illustrated (for Ar^{15+}) in figure 5 for the case of the $1s^2 2s\ ^2S_{\frac{1}{2}}$–$1s2s2p\ ^2P_{\frac{3}{2}}$ and $1s^2 2s\ ^2S_{\frac{1}{2}}$–$1s2s2p\ ^2P_{\frac{1}{2}}$ transitions, which correspond to the the q and r lines, respectively, after the notation of Gabriel (1972). The $\mathcal{PEC}$s show a clear temperature dependence.

We investigated the effect of electron density on the populations due to the inclusion of rates other than those from the ground. This is seen by a change in the ratio of the excited-state populations to the electron density. Such a deviation from a constant ratio was found at around a density of $\sim 10^{14}$ cm^{-3} for some levels, and density effects were found to be important at a density of $\sim 10^{15}$ cm^{-3} for all levels. In fusion devices, such densities are only achieved in a divertor-style regime, where the temperature is too low for the states to be populated. However, electron densities of $> 10^{14}$ cm^{-3} should be routinely generated in ITER.

Finally, we combined helium-like data (Whiteford *et al* 2001) with our present data and used the codes ADAS706 to perform parallel population calculations for the helium- and lithium-like systems and the code ADAS604 to generate synthetic spectra from these population calculations (sample spectra are shown in figure 6). These spectra include collisional-excitation processes from this work and from the work of Whiteford *et al* (2001), radiative processes (including the above-mentioned non-dipole radiative rates), dielectronic recombination and Auger decay from ADAS. The (equilibrium) ionization balance between the helium- and lithium-like systems was solved using the code ADAS405 including dielectronic recombination,

[10] We are considering a lithium-like system so these dependences are only from the ground state since there are no metastable states.

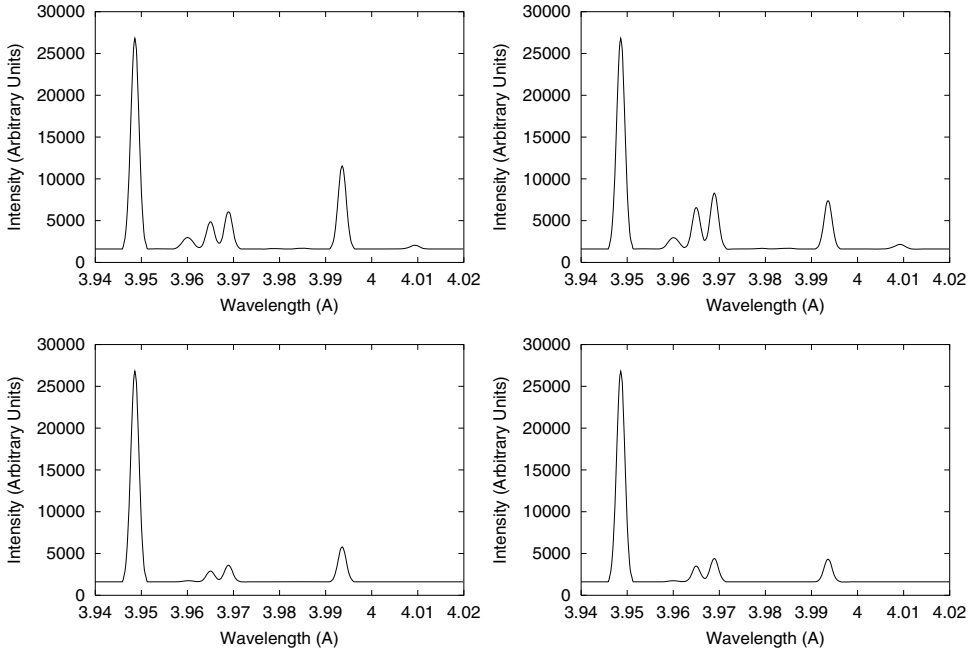

Figure 6. Ar^{16+} spectrum showing the Ar^{15+} satellite lines. The upper left plot shows the spectrum at a temperature of 8×10^6 K and density of 4×10^{12} cm^{-3}. The upper right plot shows the spectrum at a temperature of 8×10^6 K and density of 1.5×10^{15} cm^{-3}. The lower left plot shows the spectrum at a temperature of 4×10^7 K and density of 4×10^{12} cm^{-3}. The lower right plot shows the spectrum at a temperature of 4×10^7 K and density of 1.5×10^{15} cm^{-3}.

radiative recombination and collisional ionization, but excluding photoionization and three-body recombination processes. A more detailed explanation of the modelling and application will be given in a future publication.

4. Conclusions

We conclude that the present effective collision strength data are the most complete in terms of transitions, the inclusion of radiation and Auger damping, resolved resonance structure and utilization of infinite-energy limit points. The consideration of the influence of the collisional data upon excited populations increases the overall confidence in the data available for the modelling the satellite line emission required for the complete analysis of the soft x-ray spectra of helium-like ions. The methods presented here for creating and verifying collision data will serve as a benchmark for future intermediate-coupling frame transformation *R*-matrix calculations and their application to medium-to-heavy atomic mass ions.

Acknowledgments

This work was supported, in part, by a PPARC grant (PPA/G/S/1997/00783) with the University of Strathclyde. One of us (ADW) acknowledges a scholarship provided by the Caledonian Research Foundation. This work forms part of the IAEA Diagnostic CRP. We also acknowledge EPSRC grant GR/R04096 which provided the computing facilities which the calculations were

performed on (a two-node, 16-CPU, SGI Origin 300 system with a total of 12 GB of RAM and ∼1 TB of fibre channel disk[11]). We would like to thank Manuel Bautista for helpful discussions regarding the importance of Auger damping.

References

Badnell N R 1997 *J. Phys. B: At. Mol. Opt. Phys.* **30** 1–11
Badnell N R and Griffin D C 2001 *J. Phys. B: At. Mol. Opt. Phys.* **34** 681–97
Badnell N R and Pindzola M S 1993 *Phys. Rev.* A **47** 2937–42
Badnell N R and Seaton M J 1999 *J. Phys. B: At. Mol. Opt. Phys.* **32** 3955–64
Ballance C P, Badnell N R and Berrington K A 2001 *J. Phys. B: At. Mol. Opt. Phys.* **34** 3287–300
Berrington K A, Eissner W B and Norrington P H 1995 *Comput. Phys. Commun.* **92** 290–420
Berrington K A and Tully J A 1997 *Astron. Astrophys. Suppl. Ser.* **126** 105–11
Burgess A 1974 *J. Phys. B: At. Mol. Phys.* **7** L364–7
Burgess A, Chidichimo M C and Tully J A 1997 *J. Phys. B: At. Mol. Opt. Phys.* **30** 33–57
Burgess A, Hummer D G and Tully J A 1970 *Phil. Trans. R. Soc.* A **266** 225–79
Burgess A and Tully J A 1992 *Astron. Astrophys.* **254** 436–53
Burke P G and Berrington K A 1993 *Atomic and Molecular Processes—an R-Matrix Approach* (Bristol: Institute of Physics Publishing)
Burke V M, Burke P G and Scott N S 1992 *Comput. Phys. Commun.* **69** 76–98
Chen M H and Reed K J 1992 *Phys. Rev.* A **45** 4525–9
Gabriel A H 1972 *Mon. Not. R. Astron. Soc.* **160** 99–119
Goett S J and Sampson D H 1983 *At. Data Nucl. Data Tables* **29** 535–72
Goett S J, Sampson D H and Clark R E H 1984 *Astrophys. J. Suppl. Ser.* **54** 115–25
Gorczyca T W and Badnell N R 1996 *J. Phys. B: At. Mol. Opt. Phys.* **29** L283–90
Gorczyca T W and Badnell N R 2000 *J. Phys. B: At. Mol. Opt. Phys.* **33** 2511–23
Gorczyca T W and Robicheaux F 1999 *Phys. Rev.* A **60** 1216–25
Gorczyca T W, Robicheaux F, Pindzola M S and Badnell N R 1995 *Phys. Rev.* A **52** 3852–9
Gorczyca T W, Robicheaux F, Pindzola M S and Badnell N R 1996 *Phys. Rev.* A **54** 2107–15
Griffin D C, Badnell N R and Pindzola M S 1998 *J. Phys. B: At. Mol. Opt. Phys.* **31** 3713–27
Hummer D G, Berrington K A, Eissner W, Pradhan A K, Saraph H E and Tully J A 1993 *Astron. Astrophys.* **279** 298–309
Kelly R L 1987 Atomic and ionic spectrum lines below 2000 angstroms: hydrogen through krypton *J. Phys. Chem. Ref. Data* **16** suppl 1
Merts A L, Mann J B, Robb W D and Magee N H Jr 1980 *Los Alamos Report* LA-8267-MS
NIST 2001 *Atomic Spectra Database* webpage http://physics.nist.gov/
Robicheaux F, Gorczyca T W, Pindzola M S and Badnell N R 1995 *Phys. Rev.* A **52** 1319–33
Rosmej F B, Reiter D, Lisitsa V S, Bitter M, Herzog O, Bertschinger G and Kunze H-J 1999 *Plasma Phys. Control. Fusion* **41** 191–214
Sakimoto K, Terao M and Berrington K A 1990 *Phys. Rev.* A **42** 291–5
Sampson D H, Goett S J, Petrou G V, Zhang H and Clark R E H 1985a *At. Data Nucl. Data Tables* **32** 343–402
Sampson D H, Petrou G V, Goett S J and Clark R E H 1985b *At. Data Nucl. Data Tables* **32** 403–33
Summers H P 1994 *JET Joint Undertaking Report* JET-IR(94)06
Summers H P 1999 *ADAS User Manual Version 2.1* webpage http://adas.phys.strath.ac.uk/
Tayal S S and Henry R J W 1991 *Phys. Rev.* A **44** 2955–9
Whiteford A D, Badnell N R, Ballance C P, O'Mullane M G, Summers H P and Thomas A L 2001 *J. Phys. B: At. Mol. Opt. Phys.* **34** 3179–91
Zhang H L, Sampson D H and Clark R E H 1986 *Phys. Rev.* A **35** 267–318
Zhang H L, Sampson D H and Fontes C J 1990 *At. Data Nucl. Data Tables* **44** 31–70

[11] http://www.sgi.com/origin/300/